SPdKS analysis of ultralow-velocity zones beneath the western Pacific

Kevin J. Jensen,[1] Michael S. Thorne,[1] and Sebastian Rost[2]

Received 10 July 2013; revised 9 August 2013; accepted 13 August 2013.

[1] We collected a new data set of 1354 broadband SPdKS waveforms sampling the western Pacific Ocean region. These data indicate that multiple ultralow-velocity zones (ULVZs) exist in this region. We compared these data to 2.5-D synthetic seismograms computed with the PSVaxi method for a suite of 517 ULVZ models. The region beneath the North and South Philippine Sea shows no evidence for ULVZ presence. The region beneath the Coral Sea shows a large ULVZ which is approximately 700 × 700 km in lateral dimensions and up to 20 km thick. Multiple small-scale ULVZs approximately 180 × 180 km and up to 10 km thick are inferred beneath the South China Sea. Our findings are consistent with previous efforts utilizing the ScP seismic phase and provide additional constraints on ULVZ position and size. **Citation:** Jensen, K. J., M. S. Thorne, and S. Rost (2013), SPdKS analysis of ultralow-velocity zones beneath the western Pacific, *Geophys. Res. Lett.*, *40*, doi:10.1002/grl.50877.

1. Introduction

[2] Evidence for the existence of ultralow-velocity zones (ULVZs) has been put forth using seismic phases including SPdKS [e.g., *Thorne and Garnero*, 2004], PcP [e.g., *Hutko et al*., 2009], ScP [e.g., *Idehara*, 2011], ScS [*Avants et al*., 2006], PKP precursors [e.g., *Thomas et al*., 1999], SKKS/SKS amplitude ratios [*Zhang et al*., 2009], and anomalies in traveltime or slowness of a variety of different phases [e.g., *Xu and Koper*, 2009]. ULVZ physical parameters have been reported with *S* wave velocity reductions (δV_S) as large as 45% (with respect to the preliminary reference Earth model (PREM)) [*Dziewonski and Anderson*, 1981], *P* wave velocity reductions (δV_P) as large as 20%, density increases ($\delta\rho$) of up to 10%, and thicknesses (h) of up to 40 km [see *Thorne and Garnero*, 2004]. Nevertheless, strong trade-offs exist in the model space resulting in uncertainty in many of these parameters [e.g., *Garnero and Helmberger*, 1998]. At most, 40% of the surface area of the core-mantle boundary (CMB) has been probed for ULVZs [see *McNamara et al*., 2010]. The greatest concentration of ULVZs found thus far is in the central and western Pacific region and may be associated with the edges of Large Low Shear Velocity Provinces [*McNamara et al*., 2010]. However, incomplete sampling of the CMB region by seismic phases sensitive to ULVZ structure makes this assertion difficult to assess.

[3] Recent efforts have modeled SPdKS waveforms with numerical techniques in 2+ dimensions. *Rondenay et al*. [2010] utilized a 2-D pseudospectral technique and *Thorne et al*. [2013] used the 2.5-D axisymmetric finite difference approach PSVaxi. Both studies demonstrated that SPdKS waveforms are sensitive to 2-D ULVZ model geometries and that this seismic phase can be used to map ULVZ position and size. In this paper, we examine the region beneath the western Pacific Ocean using the SPdKS seismic phase and the PSVaxi modeling approach to provide better constraints on ULVZ position and size in this region. We compare these observations with ULVZs mapped in previous studies that used waveform variations of the ScP seismic phase.

2. SPdKS Data

[4] Existence of ULVZs in the western Pacific Ocean region is well established. Most of these studies have analyzed ScP [*Garnero and Vidale*, 1999; *Idehara*, 2011; *Idehara et al*., 2007; *Reasoner and Revenaugh*, 2000; *Rost and Revenaugh*, 2001; 2003; *Rost et al*., 2006; *Rost et al*., 2010; *Rost et al*., 2005] or SPdKS arrivals [*Garnero and Helmberger*, 1995; 1996; *Thorne and Garnero*, 2004; *Wen and Helmberger*, 1998]. ScP is an *S* wave that converts to a *P* wave upon reflection at the CMB (Figure 1a). SPdKS is essentially an SKS wave that strikes the CMB at the angle for critical *P* wave diffraction generating P_{diff} (*Pd*) segments along the CMB. It is assumed that any perturbation in the traveltime of SPdKS with respect to SKS is due to heterogeneity along the CMB as this is where the two raypaths diverge. Between 110° and 115°, SPdKS has been demonstrated to show the most distinctive waveform differences [*Thorne and Garnero*, 2004]; however, ULVZ signature may be observed for records as close as 105° [*Thorne et al*., 2013]. As the distance increases past 115°, SPdKS waveforms behave more similarly to those predicted by PREM. As the *Pd* path length increases, the effects of small-scale ULVZ structure are less evident. We refer to the point where *Pd* initiates along the CMB as the *Pd* inception point.

[5] Multiple ULVZs have been detected with ScP in the western Pacific Ocean region. Observations are summarized in Figure 1b. We collect broadband SPdKS data for events occurring along the Java, New Britain, Kermadec-Tonga, Ryukyu, and Marianas trenches from 1990 to 2010 with depths greater than 100 km and magnitudes $5.8 \le M_w \le 7.5$. We examined radial component data for stations from 90° to 100° epicentral distance to assess the complexity of the source-time function [see, e.g., *Thorne and Garnero*, 2004]. Events that did not possess an impulsive source-time

Additional supporting information may be found in the online version of this article.

[1]Department of Geology and Geophysics, University of Utah, Salt Lake City, Utah, USA.
[2]School of Earth and Environment, University of Leeds, Leeds, UK.

Corresponding author: M. S. Thorne, Department of Geology and Geophysics, University of Utah, Rm. 383, Frederick A. Sutton Bldg., 115 S. 1460 E., Salt Lake City, UT 84112, USA. (michael.thorne@utah.edu)

0094-8276/13/10.1002/grl.50877

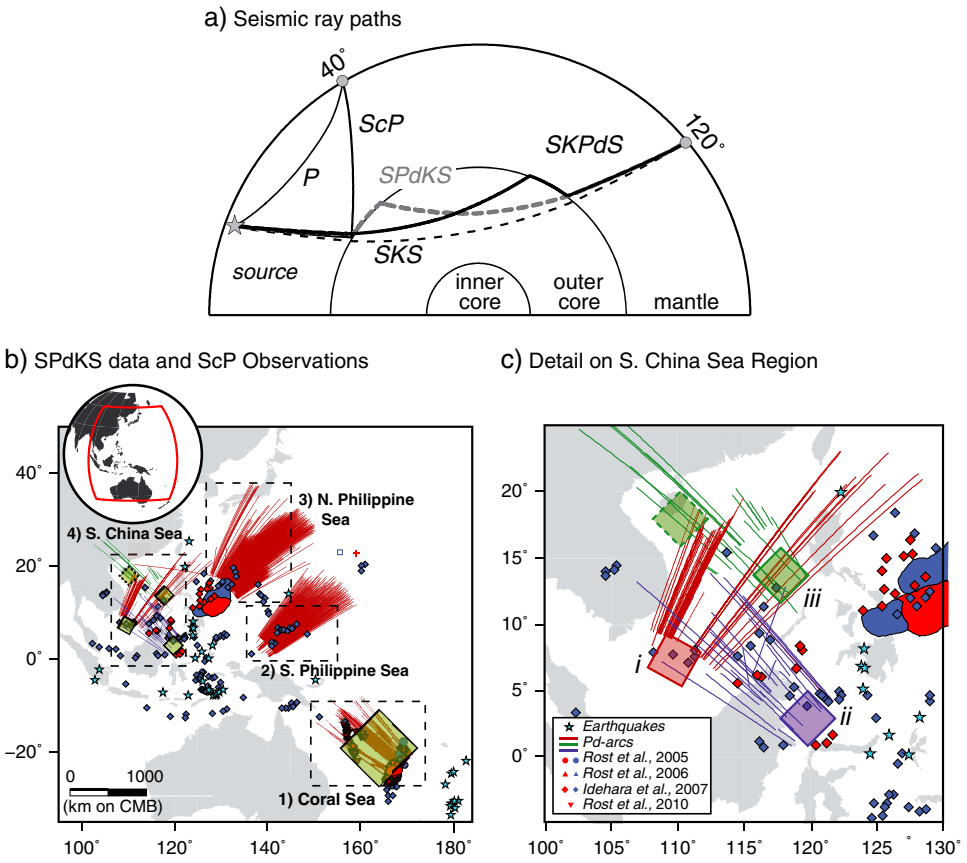

Figure 1. (a) ScP and SPdKS raypaths are shown. (b) Data used in this study were divided into four geographic regions outlined by the dashed black boxes. Red lines show the *Pd* portion along the CMB of SPdKS data collected in this study. Red (blue) diamonds, circles, and triangles show ScP bounce points on the CMB that indicate ULVZ presence (nonpresence). ULVZs mapped in this study are drawn as green shaded boxes. (c) Zoomed-in region on the South China Sea is shown. SPdKS data for this region are subset into three groups: (i) red *Pd* arcs, (ii) purple *Pd* arcs, and (iii) green *Pd* arcs.

function were discarded. After this initial quality control step, the data set included 222 earthquakes.

[6] Data were requested for these 222 events for stations between 100° and 125°. Seismograms were filtered between 0.03 and 1 Hz and visually inspected to ensure that the SKS, SKKS, and S_{diff} arrivals were identifiable and that traces were available in this distance range. Data were integrated to displacement and depth corrected to a common source depth of 500 km.

[7] We focus on four regions with excellent data coverage. Figure 1b shows the *Pd* arcs along the CMB for SPdKS data collected in the focus regions. These regions are referred to as (1) the Coral Sea, (2) the South Philippine Sea, (3) the North Philippine Sea, and (4) the South China Sea regions. Data retained include a total of 40 events with 1354 SPdKS seismograms. SPdKS data collected for two regions are shown in Figures 2a and 2c.

3. Method

[8] We calculate synthetic seismograms using the PSVaxi approach [*Thorne et al.*, 2013]. In this paper, radial component synthetic seismograms are computed for SPdKS with 6 s dominant periods, similar to that observed for this phase in broadband data. All synthetics are computed for 500 km source depth. The majority of studies have focused on the following ULVZ properties: (1) *S* wave velocity reduction (δV_S), (2) *P* wave velocity reduction (δV_P), (3) density increase ($\delta\rho$), and (4) ULVZ thickness (h). We also consider (5) ULVZ length in the great circle arc direction (*length* measured in degrees), and (6) ULVZ position (Δ_{edge}). ULVZ position (Δ_{edge}) is defined as the angular distance from the source to the source-side edge of the ULVZ. In this study, we only calculate synthetics for a density increase of +10% which is consistent with density constraints from previous efforts [e.g., *Rost et al.*, 2005], noting that minor density changes do not significantly alter the SPdKS wavefield [*Rondenay et al.*, 2010]. In total we computed synthetic seismograms for 517 unique ULVZ models (see supporting information).

[9] In order to examine geographic similarities in SPdKS waveform behavior, these data were organized into 2.5° × 2.5° geographic bins based on location of the *Pd* inception points. For each geographic bin, we generated data stacks in 1° epicentral distance bins. We compared data to synthetics by cross-correlating each data stack with the appropriate distance synthetic seismogram for each of the 517 different ULVZ models. An average cross-correlation coefficient (CCC) was calculated for each model by averaging the CCCs for each synthetic-data stack pair in each model.

[10] A consistent problem with modeling SPdKS waveforms is the significant trade-offs between model parameters [*Garnero and Helmberger*, 1998]. Many models may explain the data equally well, yet model parameters vary significantly.

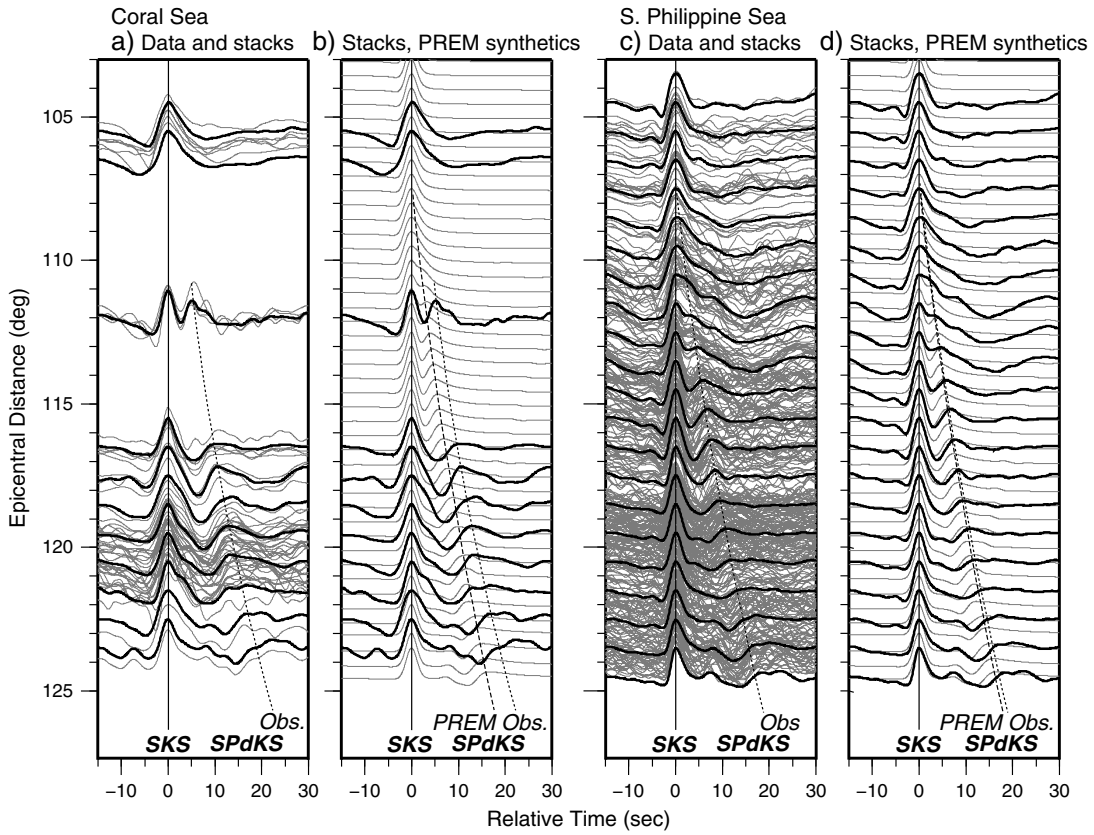

Figure 2. (a) Data observations and comparison to PREM for the Coral Sea region. In the left profile, the radial component seismograms (gray traces) are aligned on SKS with stacks (black traces) overlaying them. The right profile shows PREM synthetics overlain by data stacks aligned on SKS. (b) Same as Figure 2a but for the South Philippine Sea region.

We computed a Welch's *t* test, to compare the goodness of fit for each of the ULVZ models to the model with the highest mean CCC. For example, if the 95% confidence interval contains two models, then those models fit the data the same at least 95% of the time.

4. Results

4.1. Coral Sea Region

[11] Data for the Coral Sea region are shown in Figure 2a. There are four traces at a distance of 112° that show distinctive ULVZ-like waveforms. That is, these traces (heavy black line at 112° in Figure 2b) show the SPdKS arrival is fully bifurcated from SKS, whereas in PREM (underlying gray traces in Figure 2b), SPdKS just emerges from the shoulder of SKS. Most of the data collected in this region are recorded at long distances (116°–124°) over which the waveforms appear more PREM-like. Nevertheless, these data show a SPdKS delay with respect to PREM predictions of up to 4 s (at 124°).

[12] Comparisons of these data to synthetic predictions are summarized in Figure 3a. In general, we find that ULVZ models with large angular size (e.g., $length = 6°$ or 12°) fit these data the best. The fit degrades for models with smaller angular size ($length = 1.5°$ or 3°; supporting information). Synthetics for the best fit ULVZ model (red star in Figure 3a, model parameters: $\delta V_S = -15\%$, $\delta V_P = -5\%$, $h = 20$ km, $length = 12°$, and $\Delta_{edge} = 11.5°$) are shown overlain on data stacks in the first column of Figure 3b. The relative timing and amplitude of SPdKS with respect to SKS are well fit (avg. CCC = 0.877). However, several models explain these data equally as well (The dashed black line is drawn around those models within the 90% confidence limit.). For example, Figure 3b shows the model that fits these data third overall (green star in Figure 3a, model parameters: $\delta V_S = -45\%$, $\delta V_P = -15\%$, $h = 7.5$ km, $length = 12°$, and $\Delta_{edge} = 4.0°$) compared with data stacks (avg. CCC = 0.876). This model represents a different class of ULVZ models ($\delta V_S = -45\%$, $\delta V_P = -15\%$) than the other best fitting models ($\delta V_S = -15\%$, $\delta V_P = -5\%$). In comparing waveforms for these two models, there is little distinction between them, which exemplifies the strong modeling trade-offs inherent in SPdKS data and we cannot distinguish between models with different V_P and V_S reductions. Regardless of V_P and V_S reductions, models with angular sizes $6° \leq length \leq 12°$ provide an improved fit over those models with smaller angular sizes. The ULVZ thickness is in the range $10\text{ km} \leq h \leq 25\text{ km}$. We indicate the position and size of the best fitting ULVZ model for this region in Figure 1b (solid red box). We note that in comparing waveforms for this region to the synthetic seismograms for PREM (Figure 2b), there is a clear delay in SPdKS arrival time for these data. However, the average CCC for the PREM model (Figure 3a) is 0.803. This demonstrates the fine distinction in waveform fit for small differences in avg. CCCs and the necessity to also examine confidence intervals.

4.2. South and North Philippine Sea Regions

[13] Data for the South Philippine Sea region are shown in Figure 2c. This region has excellent data coverage and shows

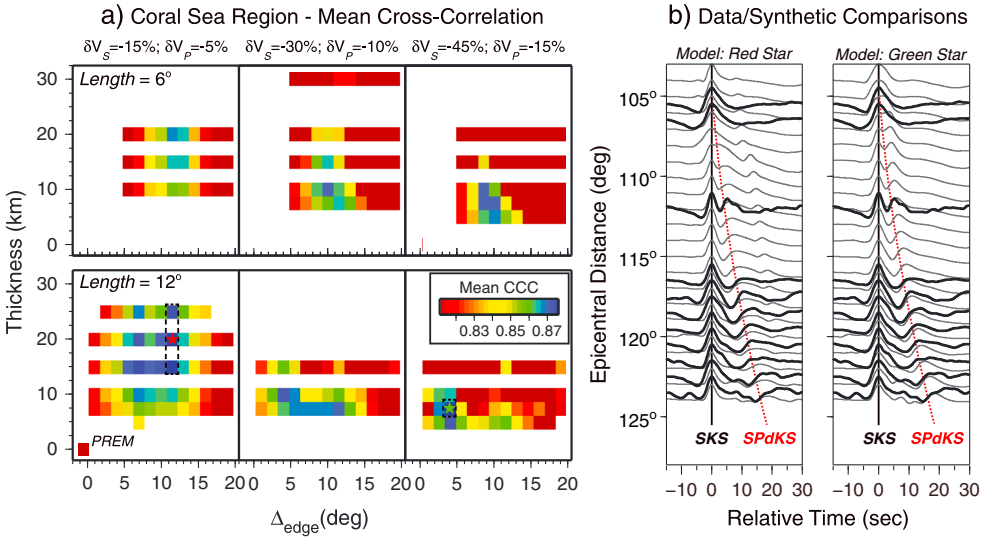

Figure 3. (a) The mean CCC between data and synthetic models for the Coral Sea Region. Top and bottom rows are for models with *lengths* = 6° and 12°. Each column is for different values of δV_S and δV_P. In each row and column, the average CCC is shown based on ULVZ thickness (h) and angular position (Δ_{edge}). The color bar is saturated at 0.81 on the low end of the CCCs. The average CCC for the PREM model is shown in lower left corner of the first plot. The best fitting model is indicated by the red star (synthetics shown in Figure 3b), and the third best fitting model is indicated by the green star (synthetics shown in Figure 3b). The dashed black line (lower left panel) shows models within the 95% confidence limit. (b) Comparison of data stacks (black traces) with synthetic seismograms (gray traces) for two models. Radial component displacement seismograms are shown aligned and normalized to unity on the SKS arrival.

remarkable similarity in waveform characteristics for each of our 2.5° × 2.5° geographic bins. Hence, for this analysis, we grouped data for all geographic bins together. The data stacks (Figure 2d) are nearly identical to PREM predictions for all distances. Minor SPdKS delays are observed (<1 s) at distances near 125°. The PREM (avg. CCC = 0.884) or ULVZ models in which SPdKS almost entirely misses the ULVZ fit these data the best, and hence we see no indication of ULVZ presence. Excellent data coverage also exists for the North Philippine Sea region. The waveforms are in excellent agreement with PREM predictions and data/model comparisons (avg. CCC = 0.881) also indicate an absence of ULVZ presence.

4.3. South China Sea Region

[14] We discuss data sampling the South China Sea region in three groups depending on *Pd*-inception point and azimuth of *Pd* arcs (see Figure 1c: bin i—red *Pd* arcs, bin ii—purple *Pd* arcs, and bin iii—green *Pd* arcs). Waveforms for bin i show good agreement with PREM predictions for distances between 112° and 125°. Some source complexity exists for one event; however, traces from 110° to 112° show SPdKS emergence with amplitude larger than SKS which is not predicted by the PREM model. The bin ii data set is sparsely populated (20 total traces), yet these waveforms show a slight delay (roughly 2 s) of SPdKS for distances between 112° and 117° (no data exist at larger distances). Bin iii traces are also sparsely populated (25 total waveforms). Two striking waveforms exist at a distance of 113° in which the SPdKS arrival is emerging from the SKS arrival. These data show broadening (possibly due to multiple overlapping arrivals) in the distance range of 108°–110° which is indicative of *Pd* inception inside a ULVZ [see, e.g., *Thorne et al*., 2013].

[15] Comparisons with synthetic predictions show that bin i data are best explained by ULVZ models with small angular size ($1.5° \le length \le 3°$). Locations in the range $10° \le \Delta_{edge} \le 11.5°$ also provide the best fits. The best fit model (avg. CCC = 0.875) has the following ULVZ characteristics: $\delta V_S = -30\%$, $\delta V_P = -10\%$, $h = 5$ km, $length = 3°$, and $\Delta_{edge} = 10.0°$. The best fit model for bin ii (avg. CCC = 0.841) is a ULVZ with the following characteristics: $\delta V_S = -45\%$, $\delta V_P = -15\%$, $h = 5$ km, $length = 3°$, and $\Delta_{edge} = 11.5°$. Models with $\delta V_S = -15\%$ and $\delta V_P = -5\%$ show a degraded fit. The CCC analysis suggests the existence of a ULVZ thickness in the range $5\text{ km} \le h \le 15\text{ km}$; angular size $1.5° \le length \le 3°$; and position $8.5° \le \Delta_{edge} \le 10°$. The comparisons between model and data for bin iii data are virtually identical to those data for bin ii. These data suggest the presence of at least one small-scale ULVZ in each data grouping.

5. Discussion and Conclusions

[16] We see no evidence of ULVZs in the North and South Philippine Sea regions. *Idehara et al*. [2007] examined these regions with ScP data, yet only a handful of observations have been made. These ScP data are consistent with our conclusion that no ULVZs exist here. *Idehara et al*. [2007] and *Idehara* [2011] both indicate a ULVZ 175 km to the southwest of our North Philippine Sea data, which is not sampled by our data.

[17] ULVZs have been indicated in the Coral Sea region [*Rost and Revenaugh*, 2001, 2003; *Rost et al*., 2010; *Rost et al*., 2005]. These studies indicate that one or more ULVZs exist with a thickness (h) averaging 9 km, inferred δV_P reductions from 5 to 8% and δV_S reductions from 22 to 25%. From these studies, it is not possible to constrain the dimensions of ULVZ(s) due to incomplete coverage (see Figure 1b). Our findings are consistent with ULVZ presence in this area; however, a larger-scale ULVZ (700 × 700 km) is indicated. Our inferred ULVZ position and size span the area in between

ULVZ sightings from *Rost et al*. [2005, 2010], suggesting that a single large ULVZ exists here. Our best fit model suggests a larger thickness (~20 km) than that previously found from ScP data (~9 km), yet we cannot rule out a thinner ULVZ due to modeling trade-offs. Regardless of ULVZ thickness, a large ULVZ (on the order of 12°) is required to match the SPdKS data. The discrepancy in thickness of the ULVZ may indicate that the ScP data are sampling thinner ULVZ edges, with the ULVZ thickening up to 20 km in the center.

[18] The South China Sea region has been probed in one study [*Idehara et al*., 2007]. These results indicate the existence of two or three ULVZs. *Idehara et al*. [2007] modeled the amplitude ratio of the postcursor phase ScSP (an ScS wave that converts to a *P* wave as it exits the ULVZ) relative to ScP which is sensitive to δV_S reductions. They conclude that δV_S reductions must be greater than 20% to account for the large amplitude ScSP postcursors observed. SPdKS data for bin i show the existence of a small ULVZ. This is not colocated with any previously observed ULVZ, but due to its small size ($h = 5$ km, $length = 3°$), it may have been challenging to detect from single ScP observations. Data for bin ii show a ULVZ in the vicinity of where *Idehara et al*. [2007] have also inferred ULVZ presence. This region is complex and may include the interaction of one or two distinct ULVZs. Our data are consistent with a ULVZ with an ~30% δV_S reduction and indicate that we likely have a thin ($h < 10$ km) and laterally small ($length \leq 3°$) ULVZ. Data for bin iii show the most direct evidence for ULVZs. In this region, we show two ULVZs. The ULVZ shown to the southeast indicates our best fitting model. Data at short distances (<110°) are indicative of a direct hit of *Pd* inception points within a ULVZ due to the existence of SPdKS precursors [*Thorne et al*., 2013]. Two anomalous waveforms observed at a distance of 112° are also indicative of a ULVZ and provide the basis for which we suggest the second ULVZ (green shaded box with dashed border). Neither of these ULVZs have been indicated in previous studies.

[19] We collected a new data set of broadband SPdKS recordings examining these data for presence/nonpresence of ULVZs. We found that data collected in the North and South Philippine Sea regions are devoid of ULVZ characteristics. However, the South China Sea and Coral Sea regions show evidence of ULVZ presence. The Coral Sea region may contain a relatively large-scale ULVZ (roughly 700×700 km). The South China Sea region is characterized by multiple small-scale ULVZs (approximately 180×180 km). Due to strong modeling trade-offs in SPdKS data, it is useful to combine these data sets and when used in conjunction, we can gain greater insight into ULVZ locations as well as reduce the uncertainty in ULVZ elastic parameters.

[20] **Acknowledgments.** We gratefully acknowledge the University of Utah Center for High Performance Computing (CHPC) for computer resources and support. We thank K. Pankow, J. Ritsema, and V. Cormier for constructive review. M.T. and K.J. were partially supported by NSF grant EAR-1014749. S.R. was partially supported by NERC grant NE/H022473/1. Figures were drawn using the Generic Mapping Tools [*Wessel and Smith*, 1998].

[21] The Editor thanks two anonymous reviewers for their assistance in evaluating this paper.

References

Avants, M., T. Lay, and E. J. Garnero (2006), A new probe of ULVZ S-wave velocity structure: Array stacking of ScS waveforms, *Geophys. Res. Lett.*, *33*, L07314, doi:10.1029/2005GL024989.

Dziewonski, A. M., and D. L. Anderson (1981), Preliminary reference Earth model, *Phys. Earth Planet. Inter.*, *25*, 297–356.

Garnero, E. J., and D. V. Helmberger (1995), A very slow basal layer underlying large-scale low-velocity anomalies in the lower mantle beneath the Pacific: Evidence from core phases, *Phys. Earth Planet. Inter.*, *91*, 161–176.

Garnero, E. J., and D. V. Helmberger (1996), Seismic detection of a thin laterally varying boundary layer at the base of the mantle beneath the central Pacific, *Geophys. Res. Lett.*, *23*(9), 977–980.

Garnero, E. J., and D. V. Helmberger (1998), Further structural constraints and uncertainties of a thin laterally varying ultralow-velocity layer at the base of the mantle, *J. Geophys. Res.*, *103*(B6), 12,495–12,509.

Garnero, E. J., and J. E. Vidale (1999), ScP; a probe of ultralow velocity zones at the base of the mantle, *Geophys. Res. Lett.*, *26*(3), 377–380.

Hutko, A. R., T. Lay, and J. Revenaugh (2009), Localized double-array stacking analysis of PcP: D″ and ULVZ structure beneath the Cocos plate, Mexico, central Pacific, and north Pacific, *Phys. Earth Planet. Inter.*, *173*, 60–74, doi:10.1016/j.pepi.2008.11.003.

Idehara, K. (2011), Structural heterogeneity of an ultra-low-velocity zone beneath the Philippine Islands: Implications for core–mantle chemical interactions induced by massive partial melting at the bottom of the mantle, *Phys. Earth Planet. Inter.*, *184*, 80–90, doi:10.1016/j.pepi.2010.10.014.

Idehara, K., A. Yamada, and D. Zhao (2007), Seismological constraints on the ultralow velocity zones in the lowermost mantle from core-reflected waves, *Phys. Earth Planet. Inter.*, *165*, 25–46, doi:10.1016/j.pepi.2007.07.005.

McNamara, A. K., E. J. Garnero, and S. Rost (2010), Tracking deep mantle reservoirs with ultra-low velocity zones, *Earth Planet. Sci. Lett.*, *299*, 1–9, doi:10.1016/j.epsl.2010.07.042.

Reasoner, C., and J. Revenaugh (2000), ScP constraints on ultralow-velocity zone density and gradient thickness beneath the Pacific, *J. Geophys. Res.*, *105*(B12), 28,173–28,182.

Rondenay, S., V. F. Cormier, and E. M. Van Ark (2010), SKS and SPdKS sensitivity to two-dimensional ultralow-velocity zones, *J. Geophys. Res.*, *115*, B04311, doi:10.1029/2009JB006733.

Rost, S., and J. Revenaugh (2001), Seismic detection of rigid zones at the top of the core, *Science*, *294*, 1911–1914.

Rost, S., and J. Revenaugh (2003), Small-scale ultralow-velocity zone structure imaged by ScP, *J. Geophys. Res.*, *108*(B1), 2056, doi:10.1029/2001JB001627.

Rost, S., E. J. Garnero, Q. Williams, and M. Manga (2005), Seismological constraints on a possible plume root at the core-mantle boundary, *Nature*, *435*, 666–669, doi:10.1038/nature03620.

Rost, S., E. J. Garnero, and Q. Williams (2006), Fine-scale ultralow-velocity zone structure from high-frequency seismic array data, *J. Geophys. Res.*, *111*, B09310, doi:10.1029/2005JB004088.

Rost, S., E. J. Garnero, and W. Stefan (2010), Thin and intermittent ultralow-velocity zones, *J. Geophys. Res.*, *115*, B06312, doi:10.1029/2009JB006981.

Thomas, C., M. Weber, C. W. Wicks, and F. Scherbaum (1999), Small scatterers in the lower mantle observed at German broadband arrays, *J. Geophys. Res.*, *104*(B7), 15,073–15,088.

Thorne, M. S., and E. J. Garnero (2004), Inferences on ultralow-velocity zone structure from a global analysis of SPdKS waves, *J. Geophys. Res.*, *109*, B08301, doi:10.1029/2004JB003010.

Thorne, M. S., E. J. Garnero, G. Jahnke, H. Igel, and A. K. McNamara (2013), Mega ultra low velocity zone and mantle flow, *Earth Planet. Sci. Lett.*, *364*, 59–67, doi:10.1016/j.epsl.2012.12.034.

Wen, L., and D. V. Helmberger (1998), A two-dimensional P-SV hybrid method and its application to modeling localized structures near the core-mantle boundary, *J. Geophys. Res.*, *103*(B8), 17,901–17,918.

Wessel, P., and W. H. F. Smith (1998), New, improved version of Generic Mapping Tools released, *EOS Transactions*, *79*, 579–579.

Xu, Y., and K. D. Koper (2009), Detection of a ULVZ at the base of the mantle beneath the northwest Pacific, *Geophys. Res. Lett.*, *36*, L17301, doi:10.1029/2009GL039387.

Zhang, Y., J. Ritsema, and M. S. Thorne (2009), Modeling the ratios of SKKS and SKS amplitudes with ultra-low velocity zones at the core-mantle boundary, *Geophys. Res. Lett.*, *36*, L19303, doi:10.1029/2009GL040030.